



HAL
open science

Combining Photogrammetry and Subsurface Geophysics to Improve Historical Knowledge of Romanesque Churches in Normandy, France: Case Study of the Notre-Dame-du-Val Chapel

Cyrille Fauchard, Laure Aillaud, Astrid Legrand, Vincent Guilbert, Cyril Ledun, Bruno Beaucamp, Raphael Antoine

► To cite this version:

Cyrille Fauchard, Laure Aillaud, Astrid Legrand, Vincent Guilbert, Cyril Ledun, et al.. Combining Photogrammetry and Subsurface Geophysics to Improve Historical Knowledge of Romanesque Churches in Normandy, France: Case Study of the Notre-Dame-du-Val Chapel. *Archaeological Prospection*, 2024, 10.1002/arp.1957. hal-04707256

HAL Id: hal-04707256

<https://hal.science/hal-04707256v1>

Submitted on 24 Sep 2024

HAL is a multi-disciplinary open access archive for the deposit and dissemination of scientific research documents, whether they are published or not. The documents may come from teaching and research institutions in France or abroad, or from public or private research centers.

L'archive ouverte pluridisciplinaire **HAL**, est destinée au dépôt et à la diffusion de documents scientifiques de niveau recherche, publiés ou non, émanant des établissements d'enseignement et de recherche français ou étrangers, des laboratoires publics ou privés.

Combining photogrammetry and subsurface geophysics to improve historical knowledge of Romanesque churches in Normandy, France: case study of the Notre-Dame-du-Val chapel

Cyrille Fauchard^{1*}, Laure Aillaud, Astrid Legrand, Vincent Guilbert¹, Cyril Ledun¹, Bruno Beaucamp¹, Raphael Antoine¹

*Corresponding author: cyrille.fauchard@cerema.fr

¹Cerema, ENDSUM Research Team, 10 chemin de la Poudrière, CS90245, F-76121 Le Grand-Quevilly, France

²EOST – École et Observatoire des Sciences de la Terre, Université de Strasbourg and CNRS, Bâtiment Descartes, 5 rue René Descartes, F-67084 Strasbourg CEDEX, France

³Université de Rouen Normandie, IUT de Rouen, Building A – 1st floor, rue Lavoisier, 76130 Mont-Saint-Aignan, France

Abstract

This study presents the results of aerial and geophysical measurements carried out on the Notre-Dame-du-Val chapel in Sotteville-sur-Mer (Normandy, France). A former leprosarium dating from the 15th century, the chapel is now deconsecrated and has been showing signs of ageing in recent years. Restoration work is planned and geophysical investigations of the area around the chapel have been commissioned. In this article, we propose a robust methodology combining aerial and terrestrial measurements in the visible range with surface prospecting methods. Compiling all the measurements within a perfectly georeferenced 3D model allows the joint analysis of the results of different physical measurement methods to provide unexpected architectural and archaeological information.

31 Photos were taken from the ground and using a drone to build photogrammetric models of the
32 interior and exterior of the chapel. Ground penetrating radar (GPR) and electrical resistivity
33 tomography (ERT) were the two survey methods deployed in the area surrounding the chapel.
34 The geophysical measurements clearly reveal traces of apses – which have now disappeared – at
35 the crossing of what would have been the building's transept, which match up with the filled-in
36 openings that are present. The existence of these apses can only be assumed from inside the
37 chapel. The resistivity anomalies are perfectly correlated with the radar anomalies and allow new
38 hypotheses to be formulated about the original structure of the chapel. Finally, mapping the local
39 geology of the surroundings based on a geophysical survey provides crucial information about the
40 history of the church's construction. Bringing this unknown architectural element to light and
41 carrying out precise mapping of the local geology surrounding the chapel constitute a major
42 breakthrough, as this will make it possible to improve our knowledge of the history of the chapel,
43 in particular its origins, through research based on archaeological surveys.

44
45 **Keywords:** Chapel, Ground Penetrating Radar, Electrical Resistivity Tomography,
46 Photogrammetry

47
48 **1 Introduction**

49
50 Subsurface geophysical prospecting involves imaging the near subsoil, generally non-
51 destructively, using physical measurement methods (Telford et al., 1990). In the field of
52 archaeological geophysics, the aim is to obtain internal images of the soil and structures that bear

53 witness to a history that has now disappeared. Geophysical methods can then be used to better
54 target excavations where geophysical anomalies are detected (Papadopoulos et al., 2014; Welc
55 et al., 2017). The old foundations of buildings, often close to the surface, generally present a
56 physical contrast that can be detected by a number of methods. In particular, multi-channel
57 ground penetrating radar (GPR) is now a widely used method for prospecting large areas because
58 the dielectric contrast between the rocky materials of the foundations and the surrounding soil
59 (topsoil, or sandy or loamy materials) is often very favourable (Bianchini Ciampoli et al., 2023;
60 Fauchard et al., 2018; Leucci, 2002; Malfitana et al., 2015; Trinks et al., 2018; Wilken et al., 2023,
61 2019). Magnetic methods (MM) are also widely used to produce maps of large areas and to image
62 near-surface anomalies (Gibson and George, 2006; Mojica et al., 2014; Tabbagh, 2018) such as
63 old foundations and traces of human activity. In most surveys, it is often the combination of
64 several methods that contributes to the quality of prospecting. For instance, high-efficiency
65 electrical methods (automated resistivity profiling (ARP)) can be complementary to GPR and MM
66 (Dabas and Ollivier, 2021; Panissod et al., 1998). Methods with lower output, but accurate
67 imaging, are often used to complement the former methods. These include electrical resistivity
68 tomography (Evangelista et al., 2017; Fabian Welc, 2017; Papadopoulos et al., 2010; Ranieri et al.,
69 2016; Tsokas et al., 2008), seismic methods (reflection, refraction and surface waves (Cafiso et
70 al., 2023; Papadopoulos et al., 2012) and microgravimetry (Batayneh et al., 2007; Panisova et al.,
71 2016, 2013, 2012; Pašteka and Zahorec, 2000; Rabbel et al., 2015). Finally, the development of
72 drones and their ability to take high-resolution photos has made it possible in recent years to
73 build 3D models of landscapes, civil engineering structures and housing, based on
74 photogrammetry (Antoine et al., 2020; Dubbini et al., 2016; Giordan et al., 2020). Combined with

75 accurate georeferencing, these models are now being used to enhance mapping and reconstruct
76 and interpret geophysical measurements in a way that is highly explicit for archaeology (Fauchard
77 et al., 2018).

78
79 In this work, we propose a robust methodology combining remote sensing and terrestrial
80 geophysical methods. Many articles in geoarchaeology are based on the combined use of
81 photogrammetry and geophysical imaging (Cooper et al., 2023; Fauchard et al., 2023; Giordan et
82 al., 2020; Guilbert et al., 2020; Linck et al., 2023; Malfitana et al., 2015; Pomar et al., 2023; Viberg
83 et al., 2013). We study the surroundings of the Notre-Dame-du-Val chapel in Sotteville-sur-Mer
84 (Normandy, France) and we clearly describe the methodology that leads to high-quality
85 visualisation and which brings to light previously unknown architectural aspects. The main
86 geophysical methods used were terrestrial and drone photogrammetry, as well as GPR and ERT.
87 The chapel is currently undergoing a restoration programme: repairs to the building are planned
88 and it is possible that conventual buildings were built in the immediate vicinity of the chapel. The
89 aim is therefore (1) to carry out a geophysical survey of the area around the chapel and (2) to find
90 potential remains of any architectural features adjoining the chapel and conventual buildings.

91
92 In the first part, the geological and historical context of the chapel is presented. In the second
93 part, the proposed methodology is described. Images taken from the ground and by drone are
94 used to produce 3D photogrammetric models of the interior and exterior of the chapel
95 respectively. In the third part, the geophysical results are given and integrated into the 3D
96 photogrammetric model. Firstly, the GPR used for the survey is a multi-channel device. It has

97 several bow-tie antennas in contact with the ground, enabling the dielectric contrasts of the
98 subsoil to be imaged in three dimensions. Secondly, ERT is used with dipole-dipole protocols to
99 image the subsurface and the distribution of its materials according to their resistivity. This
100 complements radar measurements and offers greater depth of investigation. Correlations
101 between the architectural structures of photogrammetric models and geophysical anomalies lead
102 to new interpretations. They enrich the historical analysis of the chapel, about which little has
103 been known until now, and whose archives do not mention some of the features discovered here.
104

105 **2 Local geology and history of the Notre-Dame-du-Val chapel**

106

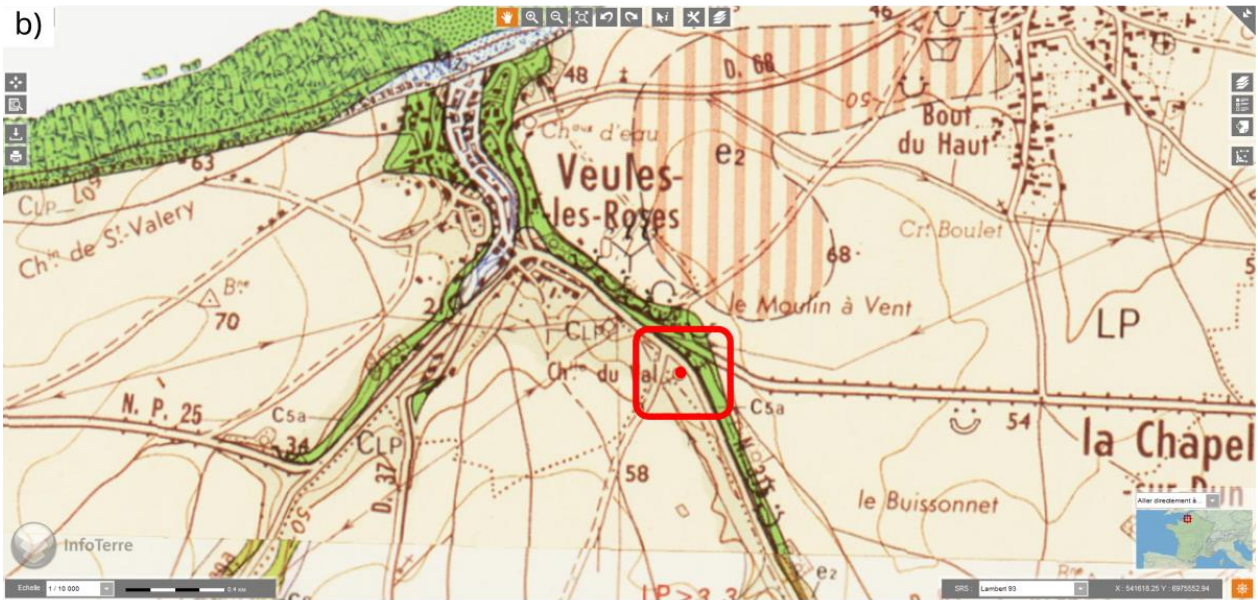
107 The Notre-Dame-du-Val chapel is located in Sotteville-sur-Mer in Normandy (France), on the
108 limestone plateau of the Pays de Caux (see Figure 1(a)). It lies slightly below a small valley. Visual
109 inspection shows that the surface of the ground surrounding the building is between 0.8 and 1 m
110 higher than the surface of the floor of the nave. It can therefore be assumed that the soil was
111 excavated to establish the chapel on a base with greater mechanical stability than the surface
112 formation. The staircase leading down to the church entrance also demonstrates this
113 construction characteristic.

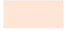



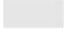


114

115 The local geology is shown in Figure 1(b). The chapel is located on loess (LP; Figure 1(c)). It is very
116 likely that the Santonian limestone formation, shown in green on the geological map on the other
117 side of the road from the chapel, lies beneath the colluvium, as revealed by archaeological
118 excavations in 1993 (Fajon, 1993; see Section 3).

119 This type of soil makes it easy to use electrical methods, which allow the subsoil to be surveyed

120 across a wide range of resistivity values. If the resistivity is lower than $100 \Omega.m$, then the depth
121 of penetration of the GPR method may be limited.
122



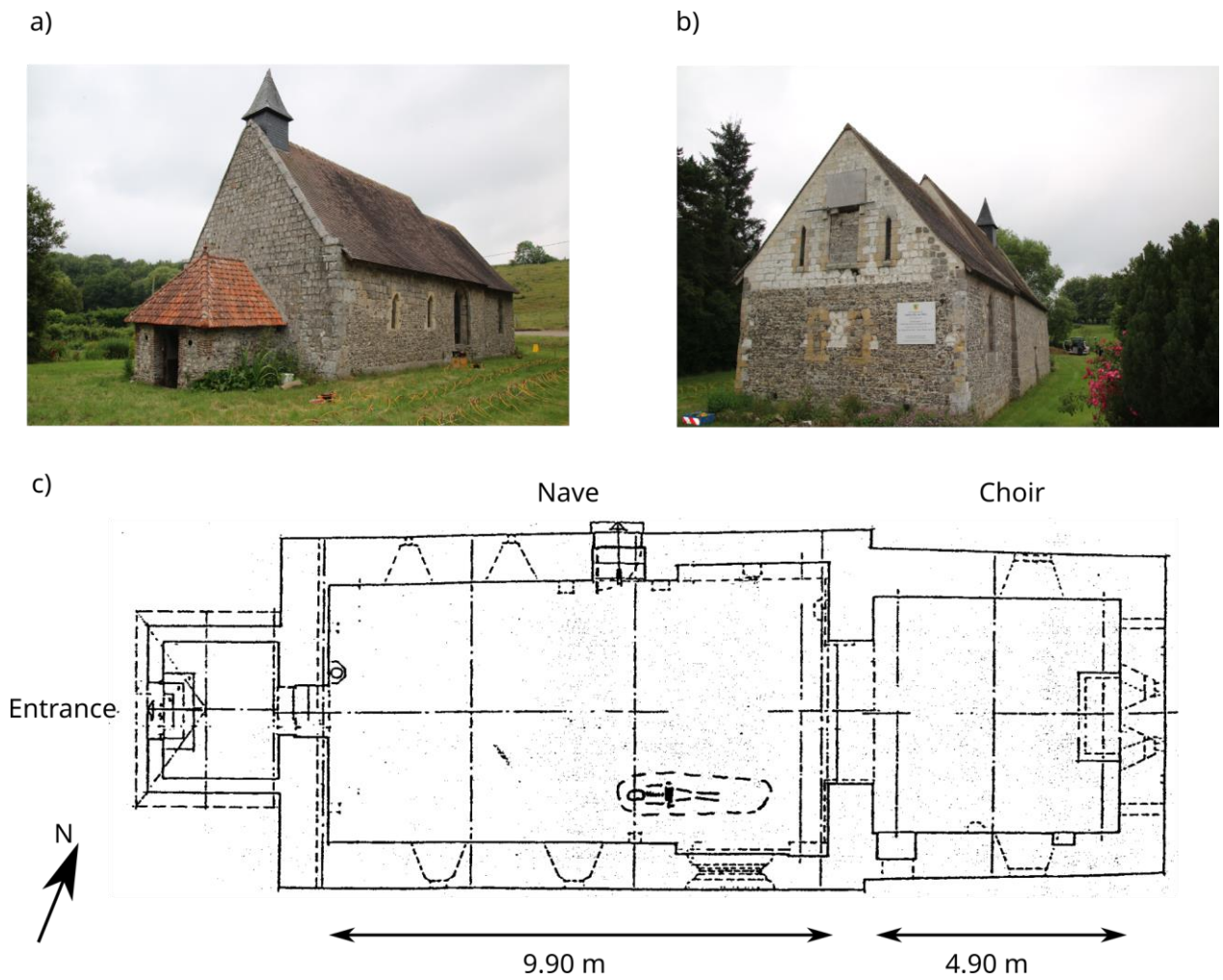
- c)
- | | |
|---|---|
|  LP - loess |  C6 - Campanian: white chalk with flints |
|  e2 - Thanetian: sands | Subdivision based on studies of foraminifera (d,e) |
|  e4 - Lower Cuisian: Varengeville formation | |
|  Fz - Quaternary: recent alluvium |  C5 - Santonian: white chalk with flints |
|  e3 - Sparnacian: sand and clay with ostracodes et molluscs, flinty clay | Subdivision based on studies of foraminifera (d,e,f) |

123

124 Figure 1: (a) Geographical location of Notre-Dame-du-Val chapel (Sotteville-sur-Mer, Normandy,

125 France); (b) detail showing local geology (1/10,000) from the 1/50,000 printed geological map;
126 (c) geological legend (source: <https://infoterre.brgm.fr/>).

127
128
129



130
131 Figure 2: Views looking (a) north and (b) south over the Notre-Dame-du-Val chapel (Sotteville-
132 sur-Mer, Normandy, France); (c) plan of the chapel (Fajon, 1993).

133
134 The current plan of the chapel is shown in Figure 2(c) and is a reproduction of the work by Fajon

135 (1993). The chapel consists of a single nave, 9.90 m long, narrowing by 30 cm on each side to form
136 the choir of the chapel, which is a square measuring 4.90 m on each side. Note the absence of a
137 transept, which usually crosses the nave of a church at right angles to give the form of a Latin
138 cross when seen from above. The chapel here contains the two main parts of a Romanesque
139 church: a nave and a choir.

140 Analysis of the soil levels from the 1993 archaeological prospection provides important
141 information for interpreting our geophysical measurements. Underneath the sandstone and flint
142 paving of the nave and the choir, the soil was identified as containing weathered limestone
143 corresponding to the Santonian limestone layer. We also note the presence of human remains
144 buried at a depth of 1.1 m to the south of the nave, probably someone in the service of the chapel.
145 The main difficulty is that there are very few written sources relating to the Notre-Dame-du-Val
146 chapel in Sotteville-sur-Mer. Only the work of Fajon (1993) sheds light on the history of the
147 building. Other historical elements can be deduced from meticulous archival research, as carried
148 out by Desriaux (2018). The exact date of construction of the Notre-Dame-du-Val chapel (see
149 Figure 2(a) and (b)) and the leprosarium (medieval leper hospital) to which it belonged is not
150 known, but the first mentions appear during the 15th century (1434–1435). The chapel then
151 underwent significant alteration in the 16th and 17th centuries. The leprosarium ceased operation
152 after 1695.

153

154 **3 Results of remote sensing and geophysical survey**

155 **3.1 Methodology**

156 Our methodology (Fauchard et al., 2023; Karamitrou et al., 2021, 2020; Kvamme et al., 2019) is

157 tried and tested, with both commercial and open-source options available. It is divided into the
158 following steps:

159 1. A photographic survey is performed covering the entirety of the chapel being studied, as well
160 as its surroundings. This survey is carried out by an operator on the ground and from the air using
161 drones, with the pilot optimizing the flight to capture the necessary details in terms of surface
162 coverage, overlap and photo quality. The ground operator and drone pilot are required to record
163 images of common scenes in order to highlight the similarities between the two survey modes.

164 2. Operators check the differential global navigation satellite system (DGNSS) positions of ground
165 targets for drone flights, the correspondence with the photographic survey of the chapel interior,
166 where no DGNSS is available, and the ERT electrode positions and the GPR coordinates. This
167 requires special attention in the field to ensure high-quality data is available for interpretation.

168 3. Photos are processed with dedicated commercial or free software, to produce a
169 photogrammetric model. In this case, commercial software (Agisoft Metashape) was used, but
170 equivalent accurate 3D point clouds can also be produced using free software such as MicMac
171 (Pierrot Deseilligny and Clery, 2011; 2012). We used CloudCompare (“CloudCompare [GPL
172 software],” 2016) and Metashape to clean the 3D point cloud and to generate a 3D mesh model.

173 4. All processed geophysical data are exported in VTK format so that the photogrammetric model
174 and the geophysical data can be displayed in the same space and in the same coordinate system
175 using the ParaView freeware (Ayachit, 2015).

176

177 **3.2 Photogrammetric and geophysical measurements**

178

179 The purpose of the photographic surveys here is to obtain 3D models of the structures into which

180 the representations of the geophysical measurements can be integrated. This enables more
181 thorough analysis, facilitates results visualisation and makes it easier to identify potential
182 correlations between visible and buried structures. Prior to these surveys, a dozen
183 photogrammetric targets were placed on the ground around the chapel and their coordinates
184 were recorded using a DGNS receiver. Inside the chapel, precise measurements were taken
185 between reference points (distances between pillars or blocks of stone that are clearly
186 identifiable in the photos, heights of openings and widths of vaults) and these were geometrically
187 linked to the DGNS points at the entrance to the chapel. This stage was essential to provide a
188 reliable coordinate system for the 3D model to be produced.

189 We carried out two photo campaigns in the visible range, with an 80% overlap between
190 images:

191 - a flight at a height of 30 m over the chapel and its surroundings using a Phantom 4
192 Pro drone, during which 159 photos were taken;

193 - a photographic survey on foot around and inside the chapel, during which 164
194 photos were taken.

195 The characteristics of the camera are given in Table 1. The characteristics of the images obtained
196 in the chapel are not included because they depend on the distance between the operator and
197 the target. As this distance varies, the size of the pixels between shots is not constant. However,
198 we estimate that their size is significantly less than 1 cm (Canon 70D camera, average
199 operator/target distance of less than 5 m).

200

201

202

203

204

205 Table 1: Characteristics of the camera on board the drone used for the flight over the chapel at

206 Sotteville-sur-Mer on 18 June 2020.

	Flight on 18 June 2020, Phantom 4 Pro
Camera	Phantom 4 Pro integrated camera
Dim. (px)	5472 x 3648
Focal length	8.8 mm
Photosite size	2.4 μm
Fly height	30 m
Ground pixel size	8.2 mm
Ground image size	44.8 x 29.8 m
Overlap	80%

207

208 The areas measured using 3D radar and the layout of the electrical resistivity profiles are

209 shown in Figures 7 and 8 respectively. For the ERT, we used an ABEM Terrameter LS 2. Five

210 profiles (see Figure 3), P2 to P6, were generated at 1 m, 2 m, 3 m, 4 m and 5 m from the south-

211 east side of the chapel. Profile P1 is located 1 m from the north side. Profile P7 is oriented south-

212 east to north-west, crossing profiles P2 to P6 and partly covering the area adjoining the entrance

213 to the chapel. Profile P2 consists of 64 electrodes spaced 0.75 m apart, giving a total length of

214 47.25 m. Profiles P1 and P3 to P7 also contains 64 electrodes, spaced 0.5 m apart, giving a total

215 length of 31.50 m. The first and last electrodes were DGNSS-controlled, and the other ERT
 216 electrodes were positioned and aligned using a measuring tape and projected onto the digital
 217 elevation model (DEM) obtained by drone. The measurements were taken using a dipole-dipole
 218 protocol with the aim of achieving a good horizontal resolution to help delineate the boundaries
 219 between natural ground and backfill ground or old building foundations, for example. Here we
 220 only show sections P2, P1 and P7 using the dipole-dipole protocol. Table 2 shows the
 221 characteristics of all the profiles, including the measurement stacking and maximum error
 222 selected, the number of iterations in the L1 norm with the Res2DInv software to obtain the
 223 inverted profiles, and the associated absolute error (Err_{ABS}).

224 Table 2: Main characteristics of dipole-dipole ERT profiles.

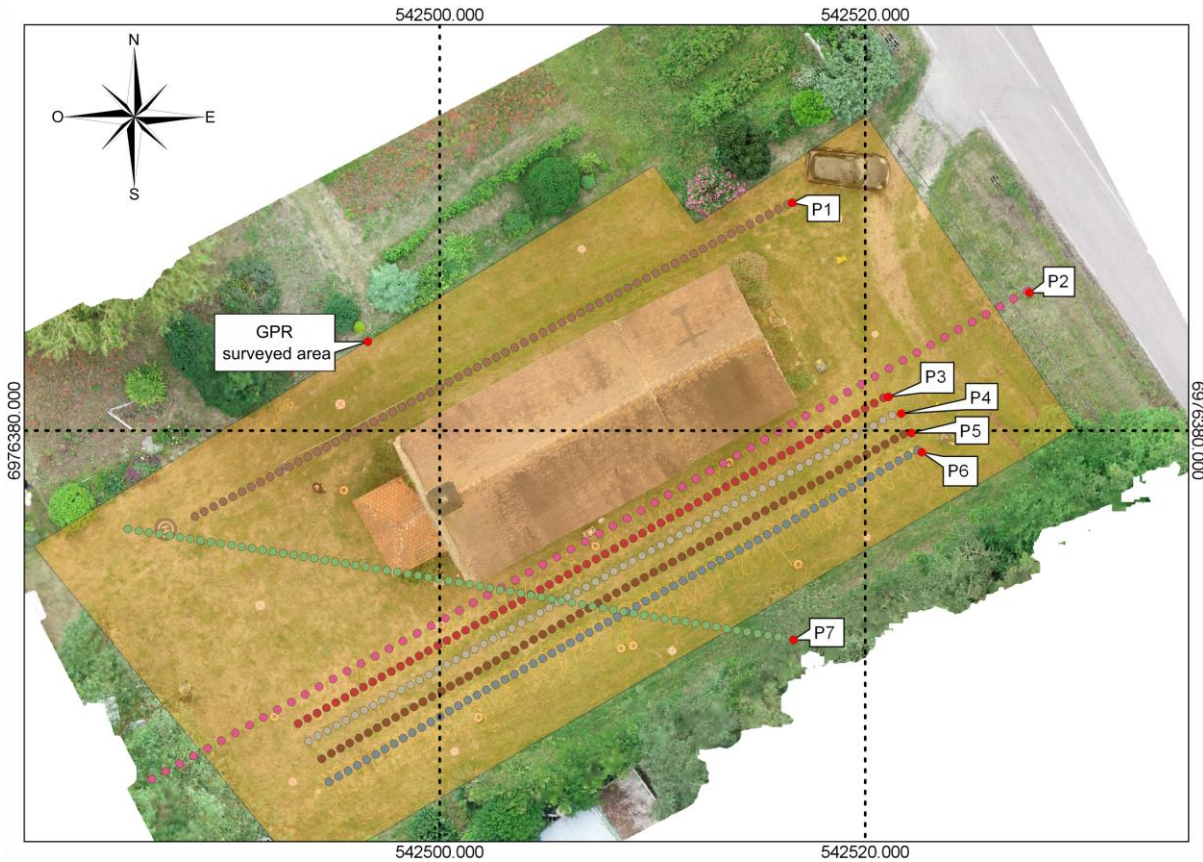
Profile	No. elec.	Spacing (m)	Length (m)	No. quadrupole	Stacking (%)	Err. var. (%) max	No. it (L1 norm)	Err_{ABS}
P1	64	0.5	31.5	1806	4	3.24	7	0.53
P2	64	0.75	47.25	1798	4	12.56	6	1.29
P3	64	0.5	31.5	1806	4	3.86	6	0.74
P4	64	0.5	31.5	1806	4	5.23	5	0.74
P5	64	0.5	31.5	1806	4	4.81	6	0.51
P6	64	0.5	31.5	1806	4	5.28	6	0.5
P7	64	0.5	31.5	1806	4	8.08	7	0.7

225
 226 For the 3D radar survey, we used the IDS Stream X pulse GPR with 8 transmitters and receivers,
 227 and bow-tie antennas in contact with the ground (ground-coupled) centred at 200 MHz in the air,

228 spread over a width of 80 cm. We obtained 7 B-scans by path (1024 samples by A-scan), with the
229 distance represented by the x coordinate; the pulse propagation time inside the subsoil, or the
230 depth if the dielectric permittivity was known, represented by the z coordinate; and the signal
231 amplitude due to dielectric contrasts shown in colour or grey scale. The dielectric permittivity is
232 in the range [4–10] for the dry loess, [10–30] for the wet loess and [7–8] for the limestone, wet
233 or dry (Telford et al., 1990). We chose an average value of 9. The value is highly dependent on the
234 distribution of materials, but, in our experience, this is a reliable value for near-surface
235 prospection using GPR in the Normandy context.

236 For 3D GPR location of profiles, the DGNSS signal sometimes deteriorates during surveys. We
237 generally prefer to delineate the zone to survey using DGNSS control points and follow a straight
238 line with a rope for the direction, with precise positioning using a measuring tape for the start
239 and end of each path. A series of signal processing phases, including move start time, background
240 removal, bandpass filter, automatic gain and migration (Sam, 2019), were applied to the
241 measured data to obtain horizontal sections (coloured maps) at a given depth z, showing the
242 surface (x,y) coordinates and the dielectric contrasts relating to the change in materials within
243 the subsoil in colour. This result is also called a C-scan. We therefore delimited the area around
244 the chapel so as to completely cover the surface in 80 cm strips.

245



246

247 Figure 3: Location of the ERT profiles (dotted lines) and the area (in yellow) investigated using

248 GPR (DGNS coordinates in Lambert 93).

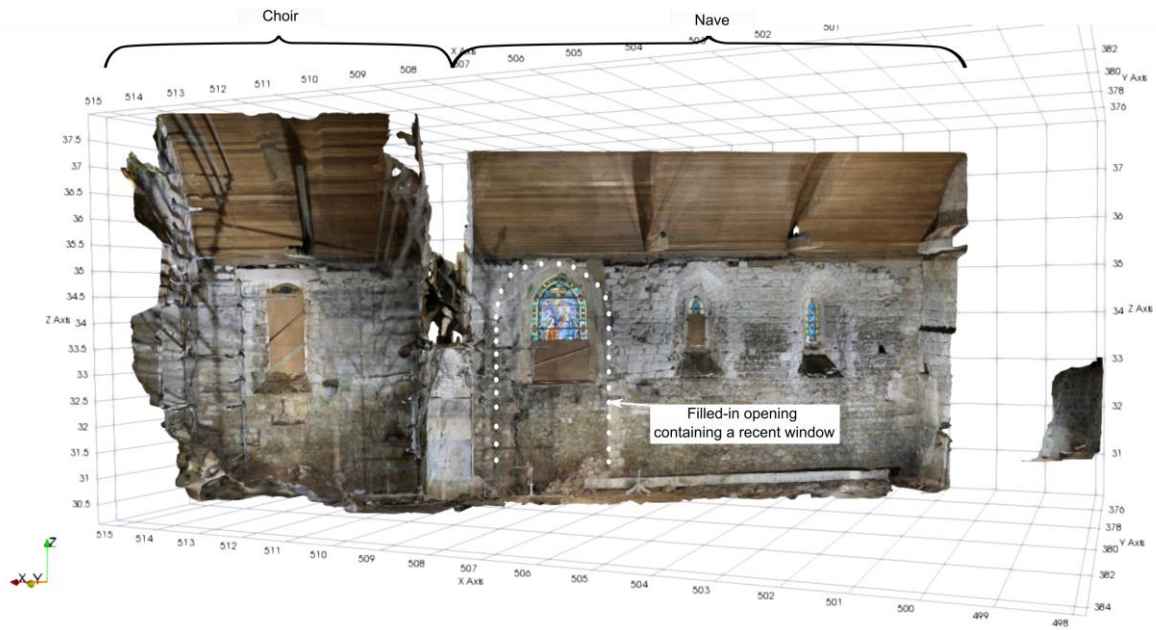
249

3.3 Results

250
251
252 To simplify the following figures, which have been produced using the ParaView software
253 (Ayachit, 2015), the local coordinates (x_i, y_i, z_i) [m] are given such that $x_i=x-542000$; $y_i=y-6976000$
254 and $z_i=z$, where (x, y, z) are the coordinates in Lambert 93 (conformal conic projection). Two 3D
255 point clouds were constructed using the Agisoft Metashape Pro photogrammetry software. The
256 exterior point cloud contained 33,017,610 points, with a resolution of 9.4 mm/px, a point density
257 of 1.13 points/cm² and a total error of 1.67 cm, and the interior point cloud 192,867,330 points,
258 with a resolution of 1.79 mm/px, a point density of 31.1 points/cm² and a total error of 2.90 cm.
259 These point clouds were then meshed to obtain a DEM of the interior and exterior of the chapel.
260 Two slices representing the interior half-DEM viewed from the north and the half-DEM viewed
261 from the south are shown in Figure 4 and Figure 5 respectively.

262
263 Firstly, the results show that photo acquisition was not optimized as there are holes in the
264 DEMs. It should be noted that the objective was not a complete internal reconstruction of the
265 architecture, but to record the main architectural elements, on the walls in particular. Secondly, the
266 interior of the chapel was not fully reconstructed due to the presence of scaffolding in part of the
267 choir and an insufficient number of photos being taken at the entrance. However, the nave was well
268 reconstructed, and it is important to highlight (i) a window (see Figure 4) in the south wall, installed
269 in a filled-in opening, and (ii) a filled-in internal arch (see Figure 5) in the north wall, both located at
270 the boundary between the nave and the choir.

271

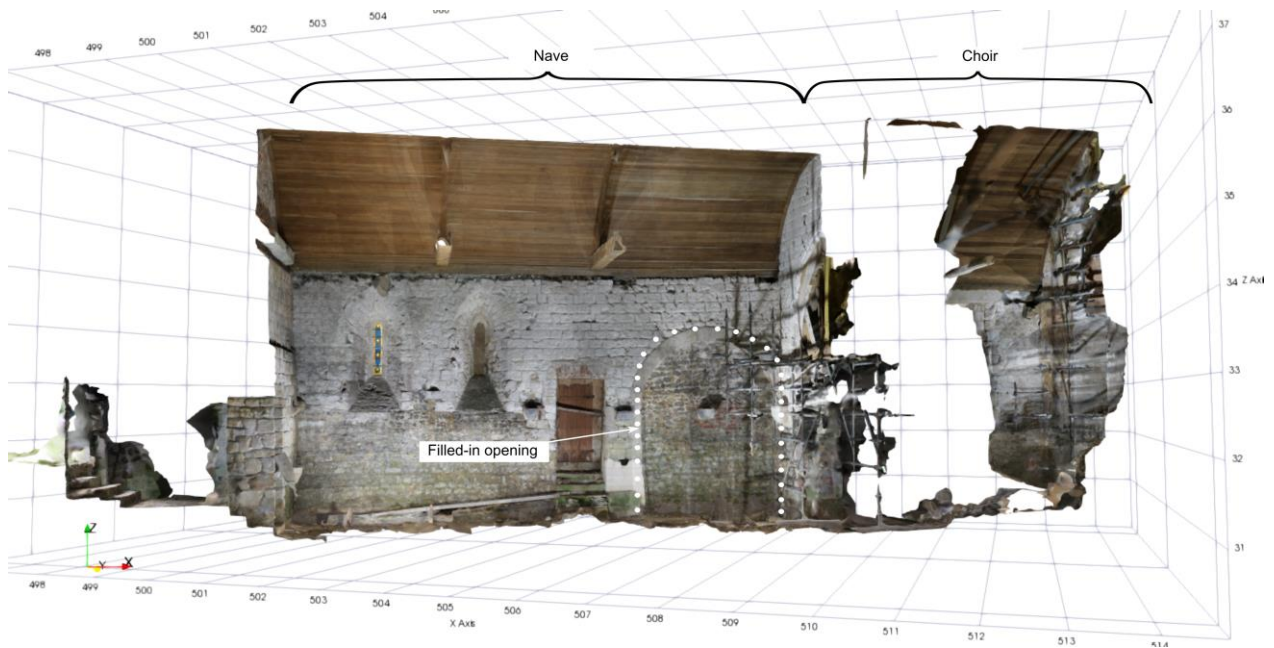


272

273 Figure 4: Half-DEM of the interior of the chapel, showing the choir, the nave and a former opening
 274 in the south wall, partly filled in with stones and stained glass.

275

276



277

278 Figure 5: Half-DEM of the interior of the chapel, showing the choir, the nave and a former

279 opening in the north wall, completely filled in with stones.

280

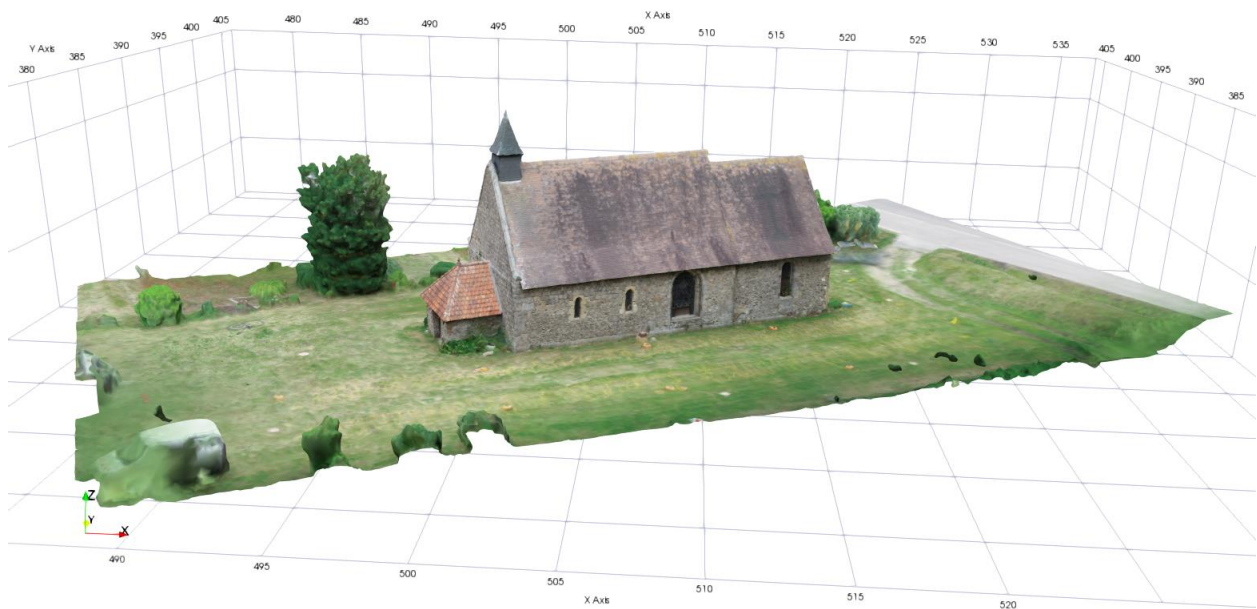
281 The external DEM is shown as viewed from the south and the north in Figure 6 and Figure 7

282 respectively. Most of the chapel and the surveyed surroundings are well represented and can

283 serve as a basis for visualising the geophysical results presented below. We notice that the filled-

284 in opening observed in Figure 5 is invisible from the outside in Figure 7, while the window of the

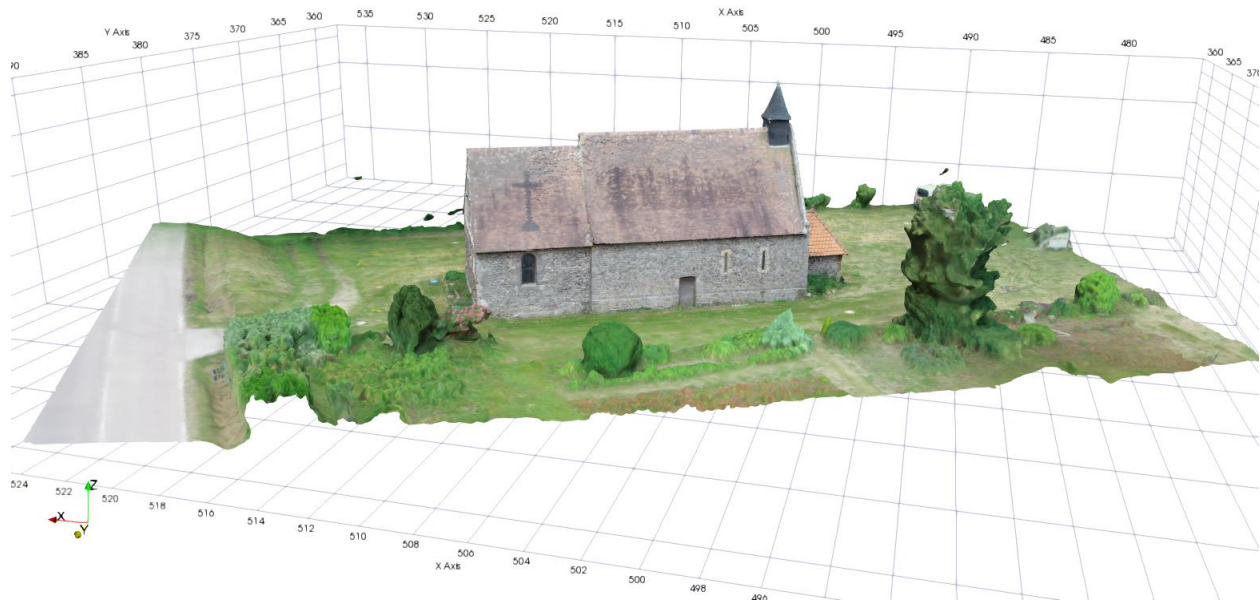
285 south wall in Figure 4 is present in Figure 6.



286

287 Figure 6: DEM of the exterior of the chapel and its surroundings, viewed from the south. The

288 partly filled former opening shown in outline in Figure 4 is visible.



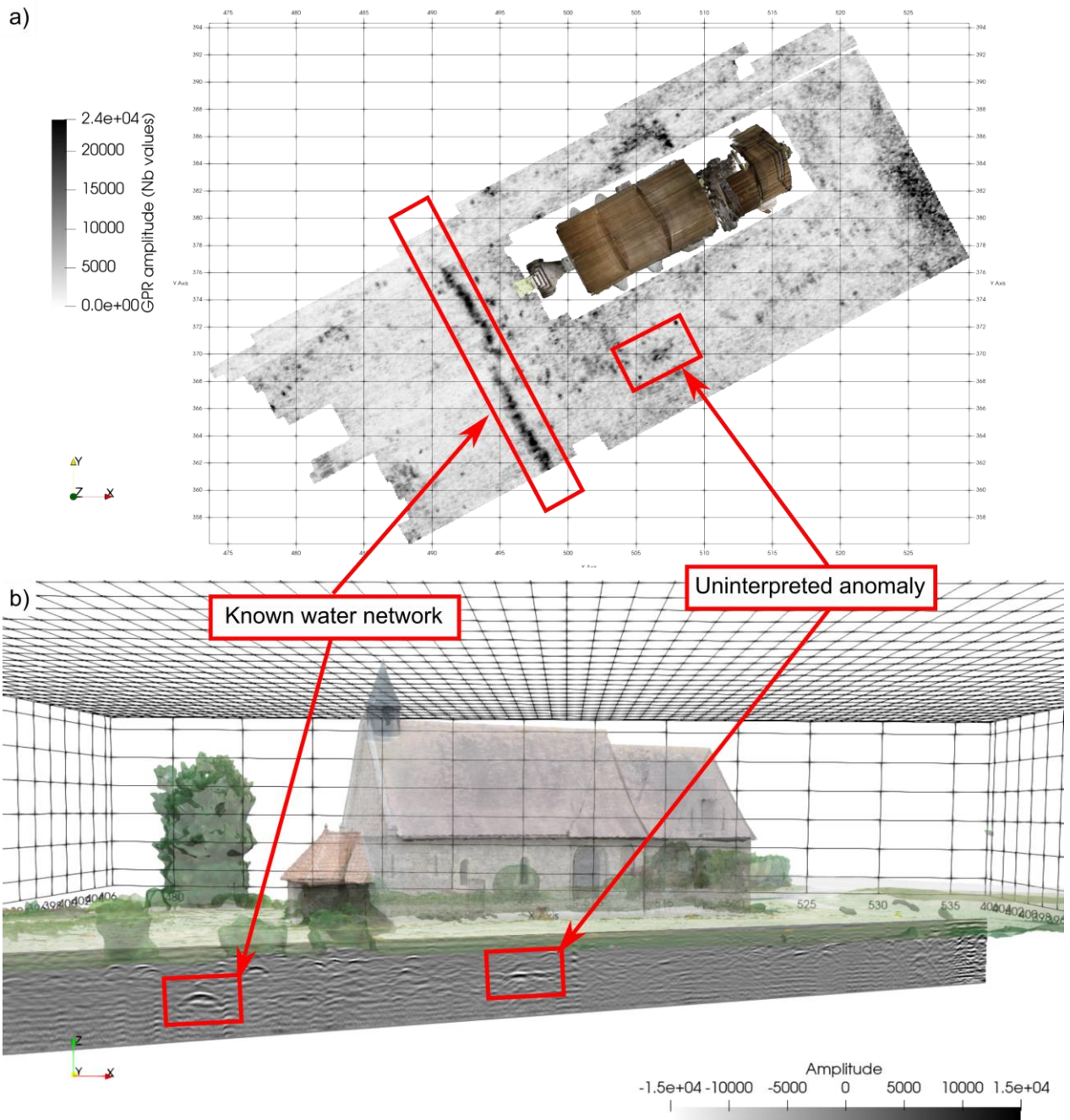
289

290 Figure 7: DEM of the exterior of the chapel and its surroundings, viewed from the north. Here,
 291 the former opening shown in Figure 5 is invisible.

292

293 The most significant C-scans are shown from an altitude of 30.75 m to 30.25 m according
 294 to the *Nivellement Général de la France* (NGF) French vertical reference system, revealing
 295 structures immediately adjacent to the chapel. The ground surface is located at 32.25 m. Figures
 296 9 to 11 clearly show ovoid underground structures starting at a depth of around 1.5 m on the
 297 south-east and north-west sides of the chapel. Their location corresponds respectively to the
 298 window built in the partly filled-in arch in the south wall and to the filled-in arch in the north wall
 299 visible only from inside the chapel (Figures 4 and 5 respectively). We can therefore assume that
 300 we have rediscovered the foundations of former apses that the chapel may have had in the past,
 301 which would have formed a transept. This is not mentioned in any archive. Figures 9 and 10 show
 302 the presence of a network running south-east to north-west (known public water network) and
 303 the very marked signature of a backfilled embankment to the north-east, close to the road.

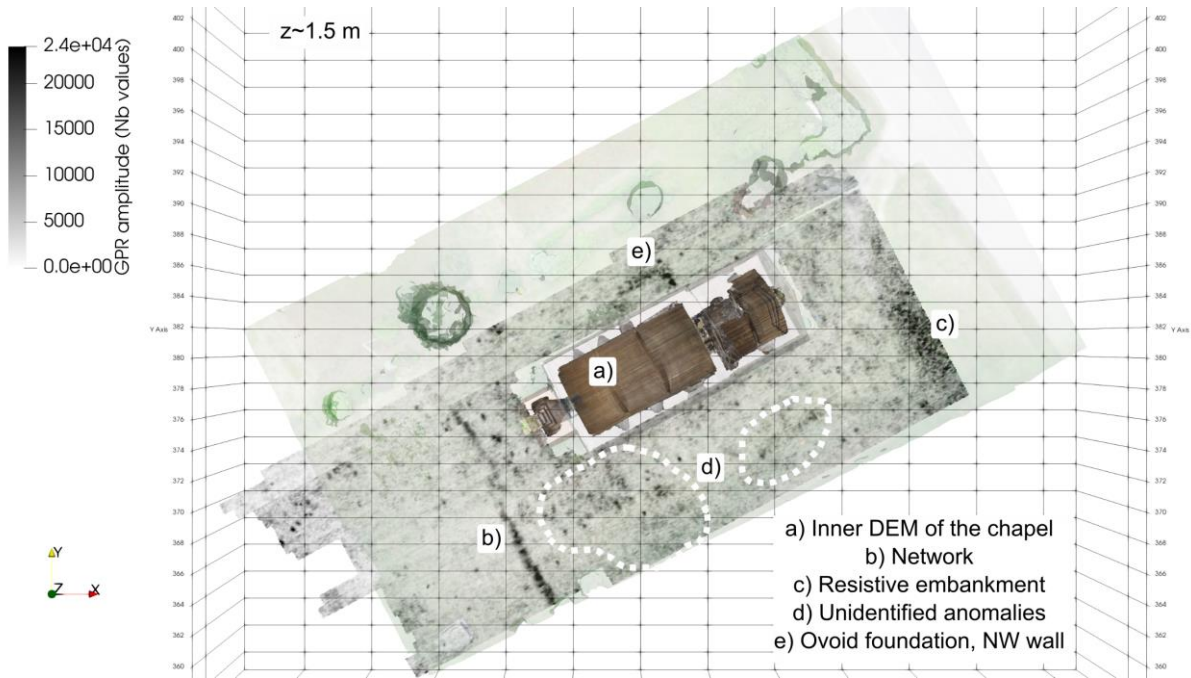
304 Numerous spot anomalies are visible, but cannot be interpreted without test excavation.
305 However, they are worth checking because, as Figure 8 shows, their radar signatures have a
306 strong contrast, which could be a sign of old foundations or graves. As shown by the ERT results
307 (see the figures 12-14), the near-surface layer corresponding to loess formation is conductive
308 enough to attenuate the electromagnetic waves such that the depth of penetration of the 3D-
309 GPR survey is about 2 m.



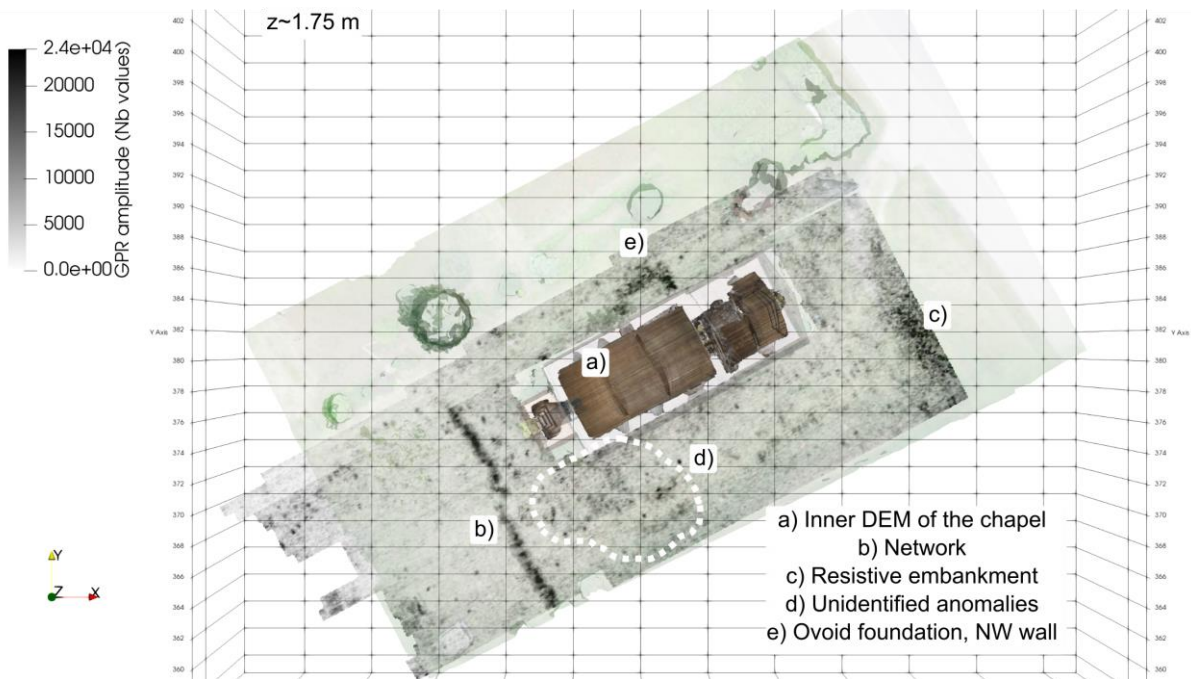
310

311 Figure 8: Example of uninterpreted anomaly meriting excavation and the signal corresponding
 312 to the known water network (a) in C-scan format and (b) in B-scan format (IDS Stream X system,
 313 central frequency of 200 MHz, width = 80 cm, 7 B-scans by path, 1024 samples by A-scan).

314

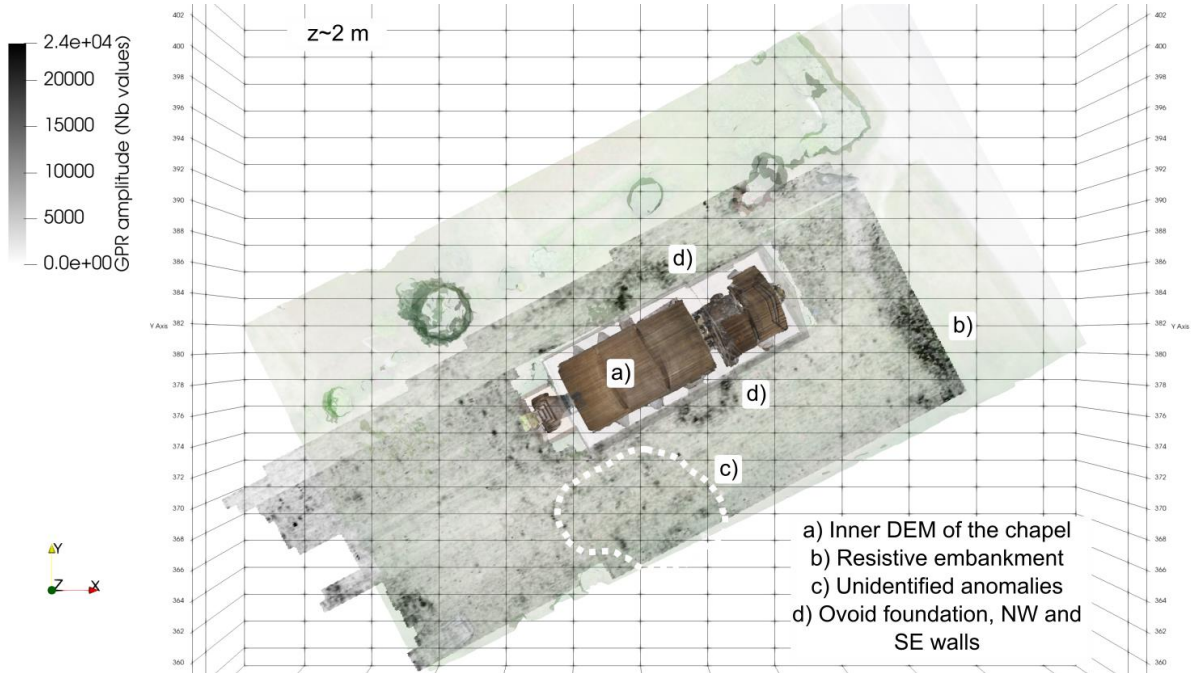


315
 316 Figure 9: Horizontal radar section (IDS Stream X system, central frequency of 200 MHz, width =
 317 80 cm, 7 B-scans by path, 1024 samples by A-scan) at a height of 30.75 m, i.e. at 1.5 m depth.



318
 319 Figure 10: Horizontal radar section (IDS Stream X system, central frequency of 200 MHz, width =
 320 80 cm, 7 B-scans by path, 1024 samples by A-scan) at a height of 30.5 m, i.e. at 1.75 m depth.

321

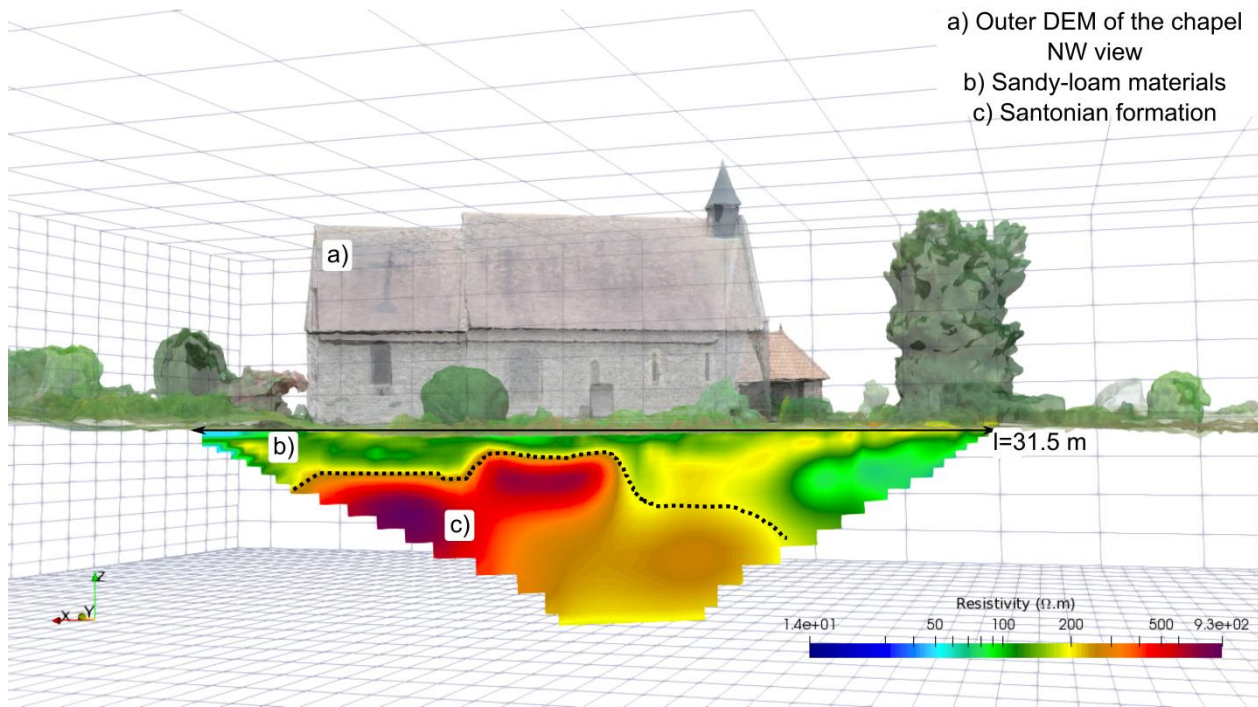


323 Figure 11: Horizontal radar section (IDS Stream X system, central frequency of 200 MHz, width =
324 80 cm, 7 B-scans by path, 1024 samples by A-scan) at a height of 30.25 m, i.e. at 2 m depth.

325

326 ERT profile P1 (see Figure 12) shows a top layer with resistivities in the order of 50–150 Ω .m
327 corresponding to topsoil and probably sandy-loam materials. Then, in the first part of the profile,
328 high resistivities can be clearly seen, possibly corresponding to the Santonian limestone
329 mentioned in Section 2, located at a depth of around 1.5 m beneath the choir of the chapel and
330 at a depth of less than 1 m at the beginning of the nave. It can be assumed that this latter part is
331 an area that was filled in to provide a foundation for the building.

332



333

334 Figure 12: Dipole-dipole ERT profile P1 (Terrameter LS 2 system, 64 electrodes, 0.5 m spacing,

335 Err = 0.53, see Table 2 for more details), 1 m from the north side of the chapel.

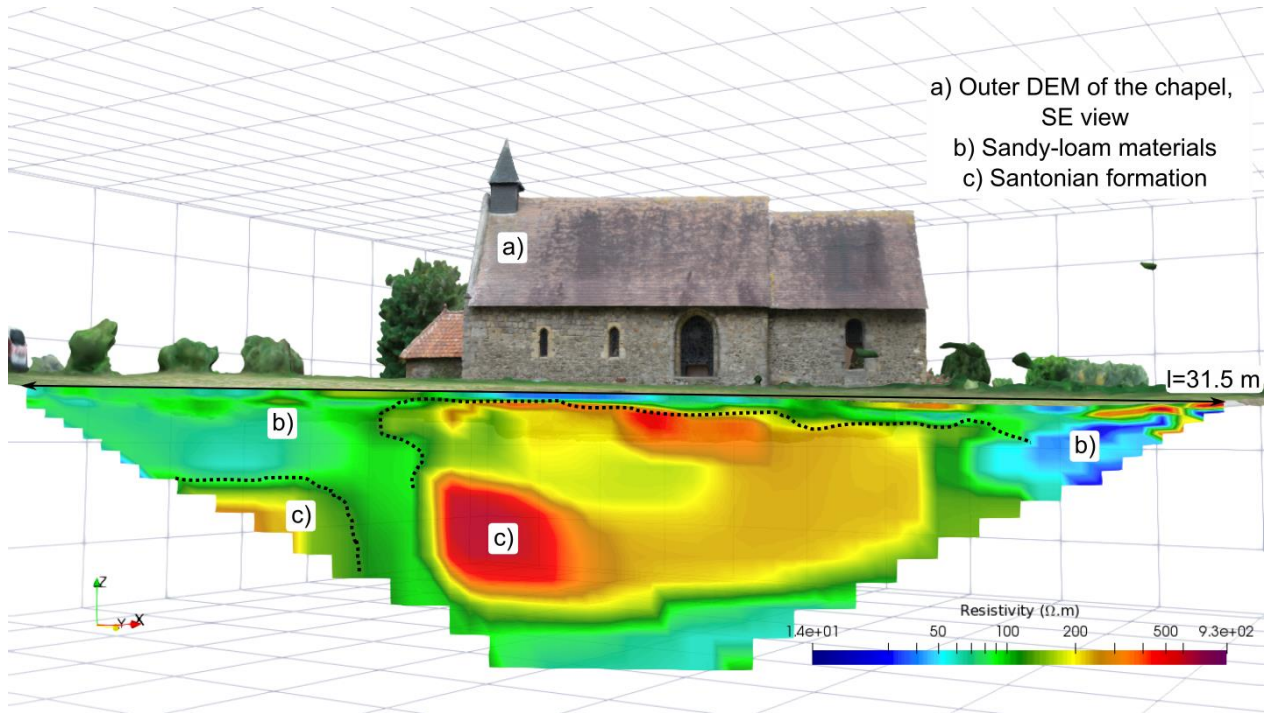
336

337 ERT profile P2, shown in Figure 13, is located along the south face. It has similar characteristics,

338 but the thickness of the top layer is less than 50 cm. Here again, there is a more resistant section

339 under the nave just before the centre of the chapel.

340



341

342 Figure 13: Dipole-dipole ERT profile P2 (Terrameter LS 2 system, 64 electrodes, 0.75 m spacing,

343 Err = 1.29, see Table 2 for more details), 1 m from the south side of the chapel.

344

345 Transverse ERT profile P7 shown in Figure 14 partly reproduces the local geology of profiles P1

346 and P2. Highly resistant anomalies can be seen in front of the church entrance; these have not

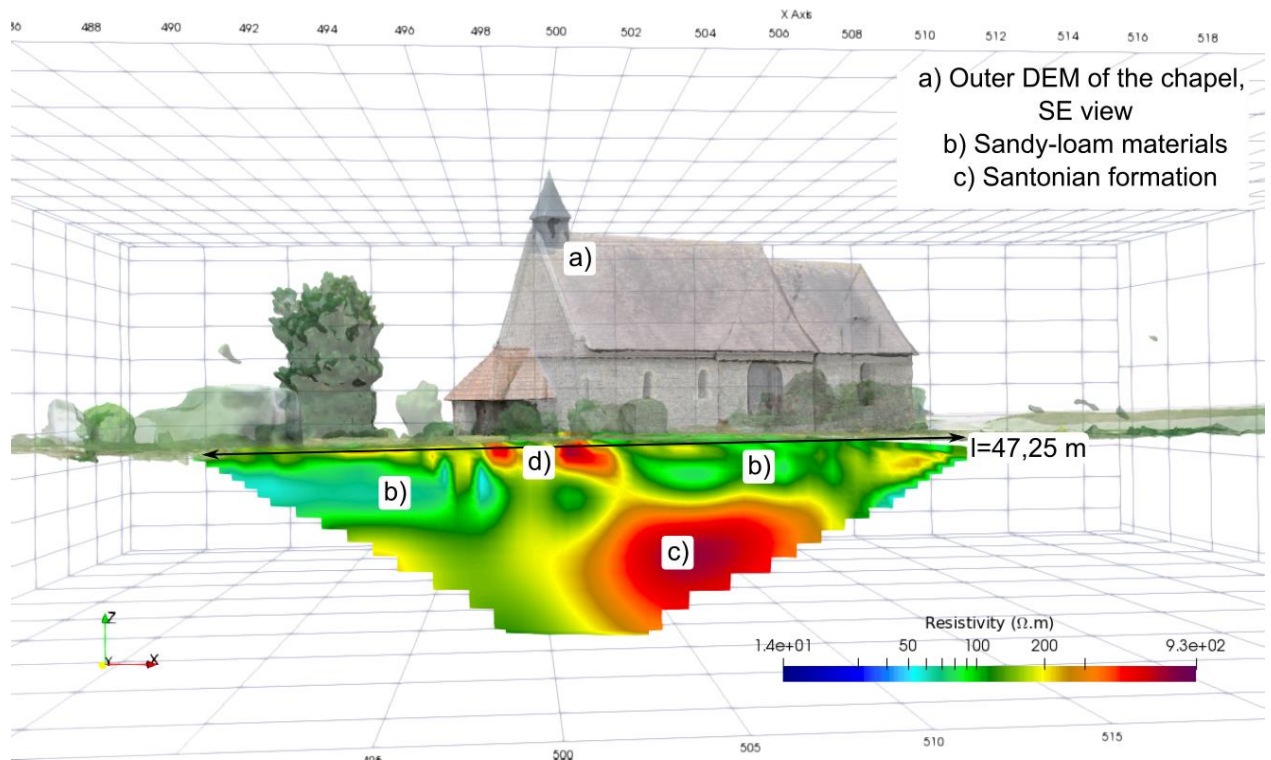
347 been interpreted. Here again, it seems that the chapel was built on very resistant soil

348 corresponding to the Santonian limestone to ensure a good foundation for the building. It is also

349 very likely that the builders had to excavate the surface layer to reach levels that were satisfactory

350 from a mechanical point of view.

351



352

353 Figure 14: Dipole-dipole ERT profile P7 (Terrameter LS 2 system, 64 electrodes, 0.5 m spacing, Err
354 = 0.7, see Table 2 for more details), south-east to north-west passing in front of the chapel
355 entrance.

356 4 Discussion and interpretation

357

358 The assessment of the Notre-Dame-du-Val chapel is based on several types of data:

- 359 - a drone photographic survey of the exterior and surrounding area;
- 360 - a terrestrial photographic survey of the interior;
- 361 - the fusion of interior and exterior DEMs produced using the photogrammetric method;

362 - 3D GPR measurements of the surrounding area;

363 - ERT measurements of the same area.

364 The DEM produced by photogrammetry with the drone provides a complete reconstruction of
365 the chapel's exterior architecture. This model can be used as a basis for future architectural
366 studies or restoration work. It is available in high definition (pixel size less than 1 cm). The interior
367 DEM is incomplete due to the presence of scaffolding on the day of the measurements. The model
368 provides a better view of the remains of former openings in the north and south walls, at the
369 transition between the nave and the choir. These openings undoubtedly led to former apses and
370 a transept, and thus gave the Latin cross shape seen from above that is associated with this type
371 of religious building.

372 This hypothesis is confirmed by geophysical measurements. Firstly, the 3D radar sections
373 clearly show the existence of semicircular foundations on the site, which appear at a depth of
374 1.5 m to 1 m on the north side and 1.5 m on the south side. These depths should be checked for
375 accuracy by drilling or excavation. The bases of these semicircular shapes correspond to the bases
376 of the arches visible on the interior model. Secondly, the ERT sections show that the builders
377 reached a stable geological horizon (the Santonian limestone), which had been revealed by earlier
378 excavations reported in former works. These geological horizons, capable of supporting the
379 weight of the building, are highlighted by the ERT measurements on profiles P1 (north facade)
380 and P2 (south facade). It should be noted that this local geological layer constitutes very resistive
381 material under the chapel and lies closer to the surface under the areas of the presumed apses.
382 It is therefore likely that backfilling work involved raising the mechanically stable layer to
383 accommodate these apses. The identification of this architectural feature is the major finding of

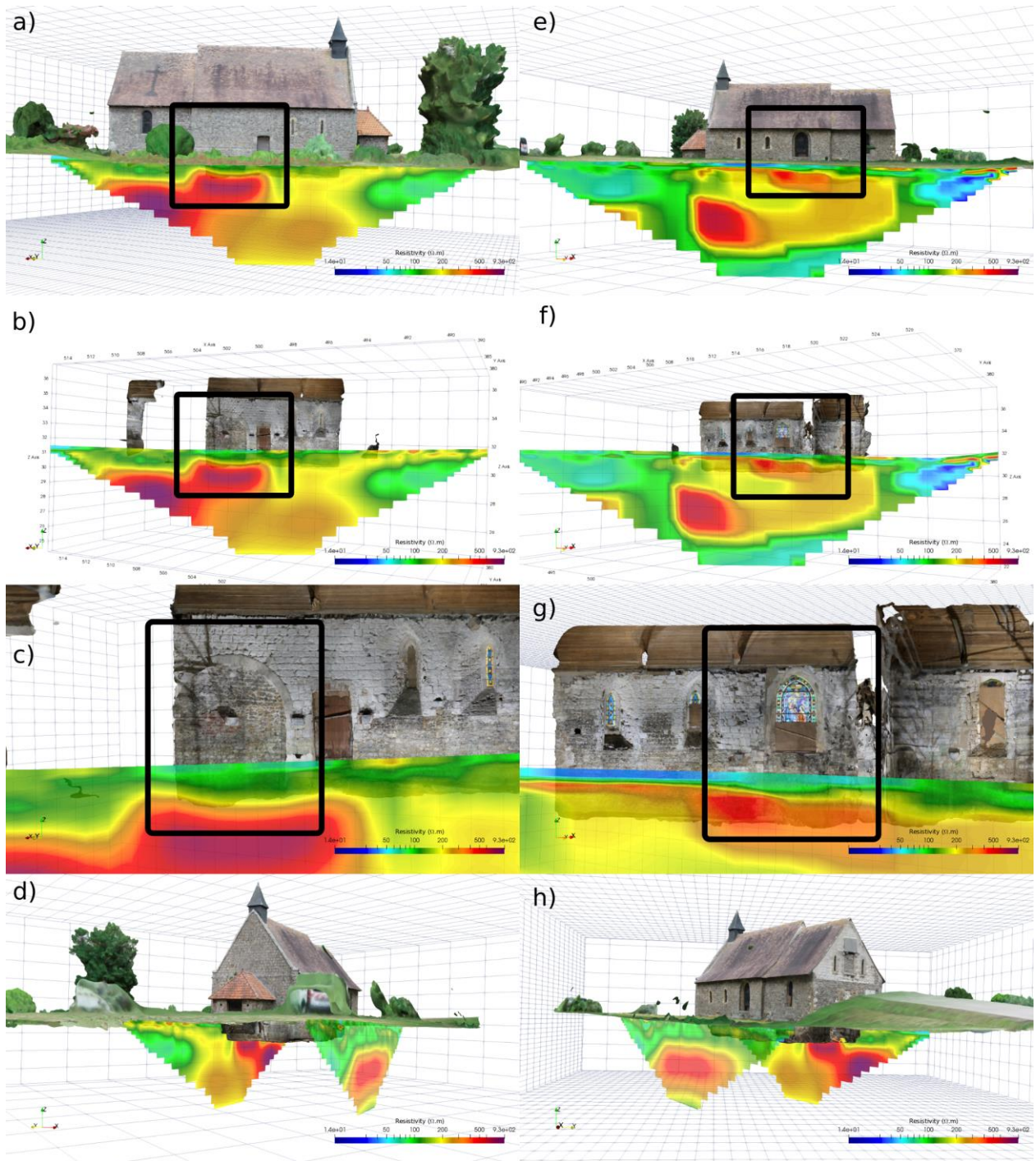
384 this archaeological survey: no previous works mention the presence of apses of the Notre-Dame-
385 du-Val chapel. The methodology under consideration based on the analysis of photogrammetry
386 and near-surface geophysics is a highly effective approach that can contribute to the historical
387 knowledge of such a building. This analysis is shown in full in Figures 15, 16 and 17.

388
389 Dating the origin of this church is a real challenge. Daoust (1969) claims that the
390 leprosarium dates back to the 12th century, but fails to cite any clear historical references. The
391 Notre-Dame-du-Val chapel is not among the leprosaria in the eastern Normandy and Vexin
392 regions listed by Eudes Rigaud, Archbishop of Rouen, in the 13th century. Yet we know today that
393 his census of leprosaria is not complete (Tabuteau, 2019). Important progress (Guibert and Sapin,
394 2010; Sapin et al., 2008) has been made in dating medieval buildings, thanks to the radiocarbon
395 dating of wood or charcoal from the mortar of old buildings. In our case, no radiocarbon dating
396 studies were performed.

397 Nevertheless, significant architectural features (Desriaux, 2018) such as the ogival chevet
398 window and the semicircular arch of the south wall suggest that it was built in the 12th or 13th
399 century. The name of a building is often linked to the period in which it was built (Wasylyszyn,
400 2006). For example, many churches from the early Middle Ages bear the name "Notre-Dame".
401 Carré et al. (2011) has studied and recorded a large number of Romanesque churches of the early
402 Middle Ages (up to the 11th century). These churches are mostly composed of a single rectangular
403 nave, extended either by a narrower choir with a flat chevet, as in the chapel of Sotteville-Sur-
404 Mer, or by a semicircular apse (Erlande-Brandenburg, 1966), "as in the church of Saint-Georges
405 at Saint-Georges-Motel. The rare transepts found in today's churches were added after the 12th

406 century, as in the churches of Saint-Martin in Coudray-en-Vexin. Only the churches of Cailly
407 (canton of Mesnil-Esnard, Seine-Maritime) and Dampierre (canton of Gournay, Seine-Maritime)
408 appear to have had a Latin cross plan" (Wasylyszyn (2018, 2006). This last remark supports the
409 analysis of the architectural elements, allowing us to estimate the origin of the chapel in the 12th
410 century. Although the Notre-Dame-du-Val chapel does not currently have a transept, the
411 geophysical results (see Section 3.3) indicate that a transept formerly existed.

412



413

414

415

416

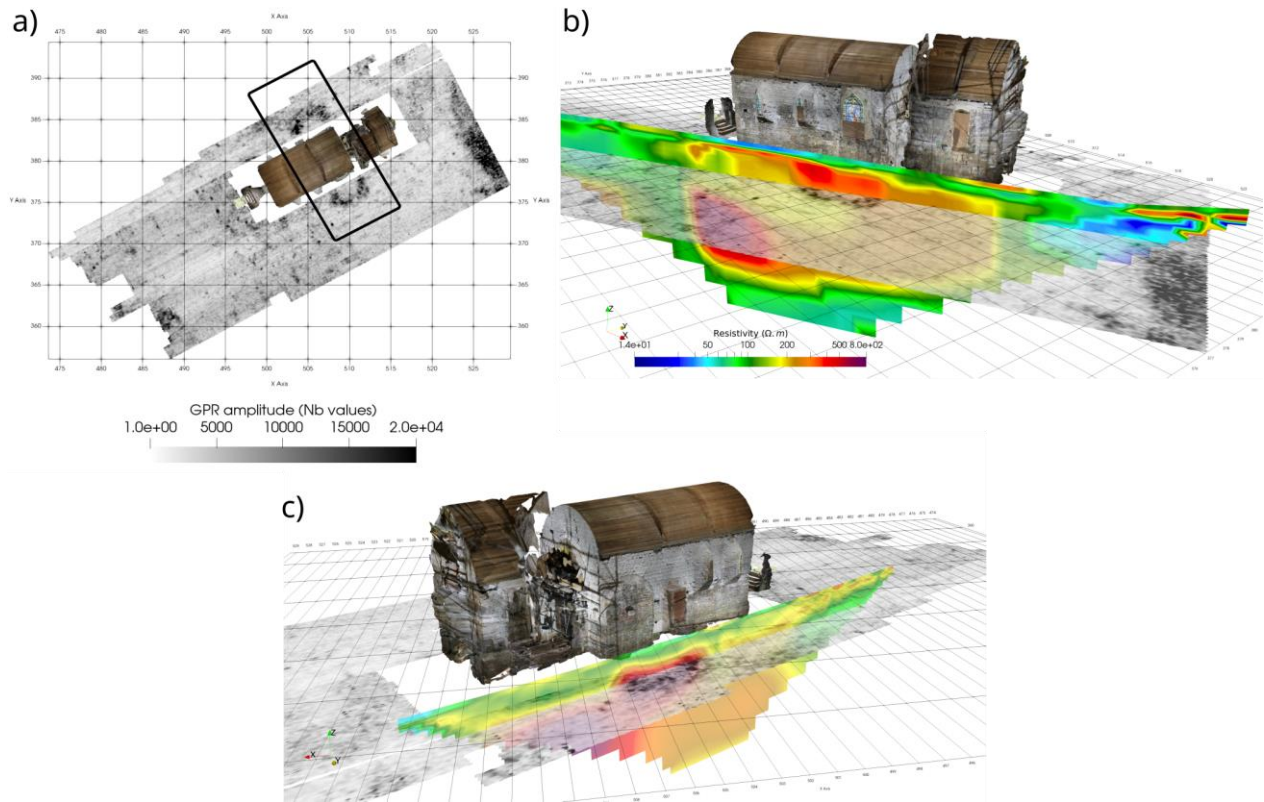
417

Figure 15: (a) ERT profile P1 with exterior DEM, and (b) with interior DEM; (e) ERT profile P2 with exterior DEM, and (f) with interior DEM. The black frame shows a raised bed in relation to the Santonian limestone level on which the north and south apses were built. In figures (c) and (g), the close-ups highlight the position of these foundations directly in line with the arches of

418 the interior DEM. Overall views (d) and (h) show the general foundations of the chapel on the
419 Santonian limestone.

420

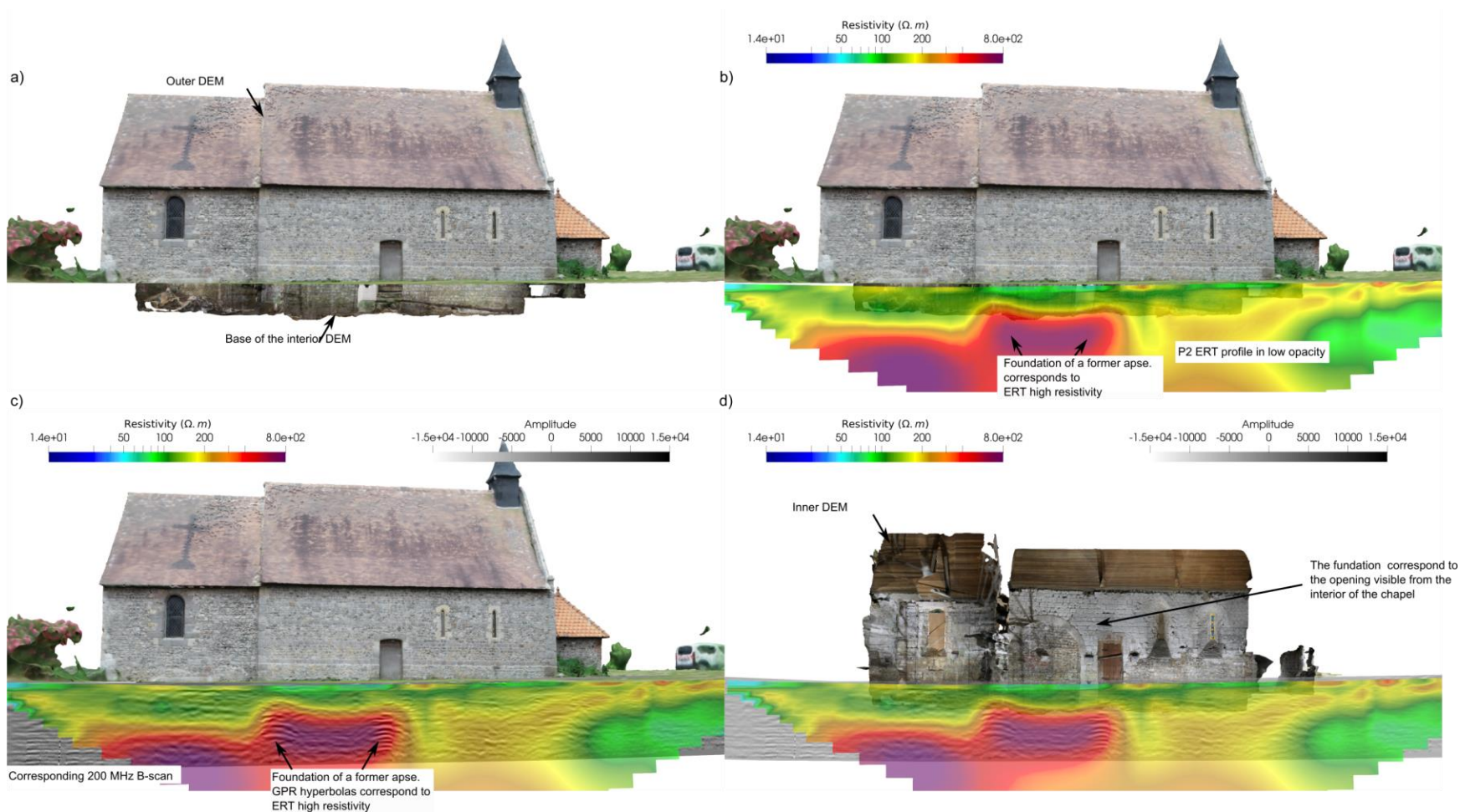
421



422

423 Figure 16: (a) C-scans at a depth of about 1.5 m, with interior DEM. The black frame highlights the
424 semicircular foundations of the north and south apses at the transition between the nave and the
425 choir. Figures (b) and (c) show the same C-scan combined with ERT profiles P2 and P1 respectively.
426 We see that the radar signal indicating the apses matches the raised level with high resistivity.

427



428
 429 Figure 17: (a) Exterior and interior DEM, (b) with ERT profile P1 and (c) with the corresponding B-scan taken 1 m from the north side
 430 of the chapel wall. The foundations of the former apses appear as hyperbolas in the B-scan and show a high resistivity (Santonian
 431 limestone) on ERT profile P1, corresponding to the former opening visible only from inside the chapel.

432

433 **5 Conclusion**

434

435 Remote sensing and geophysical surveys were carried out to clarify the architectural history of
436 the Notre-Dame-du-Val chapel in spring 2020. These surveys consisted of photographic surveys
437 of the exterior of the chapel and its surroundings using a drone, and of the interior of the building.
438 They were supplemented by 3D radar and ERT geophysical measurements carried out on the land
439 surrounding the chapel.

440 This remote sensing and geophysical campaign led to two main findings. Firstly, foundations of
441 former apses at the crossing of what would have been the transept have been revealed by
442 geophysical measurements, notably through the use of GPR. This is a major finding, as there is no
443 trace of this architectural feature in the literature. Excavation work to uncover the foundations
444 would be a great help in determining the age of the church and thus improving our historical
445 knowledge. Secondly, the Santonian formation is clearly depicted by the ERT results and explains
446 why the builders constructed the floor of the church 1 m deeper than the surrounding ground.
447 Our work also demonstrates that the overall methodology combining the use of remote sensing
448 with geophysical methods is a relevant approach for reconstructing the chapel and visualising the
449 results in 3D, in order to supplement the history of the chapel in a convincing manner. This
450 methodology, based on open-source and commercial software, can be reproduced for other
451 studies. In fact, the use of complementary geophysical methods (seismic, microgravimetry and
452 magnetometry), as well as the deployment of 3D measurement protocols (in electrical methods),
453 would represent a major step forward.

454

455

456 **6 Acknowledgements**

457

458 We would like to thank the Council of Sotteville-sur-Mer and the non-profit organisation *Pour*
459 *Que Vive La Chapelle Du Val* for their support. We would also like to thank Paul-Franck Thérain,
460 heritage engineer, who at the time of the request was working for the Seine-Maritime
461 Department of Cultural Heritage. Finally, we would like to thank Emmanuel Fajon for his
462 contribution to the work presented here, as well as Charles Le Cœur, former director of the
463 Meudon Laboratory of Physical Geography (research unit UMR 8591), who helped us clarify our
464 understanding of the local geology.

465

466 **7 Conflict of interest statement**

467 This study has no conflicts of interest.

468 **8 Data availability**

469 All the data used in this study are available on request.

470

471

472 **9 Bibliography**

473

474 Antoine, R., Lopez, T., Tanguy, M., Lissak, C., Gailler, L., Labazuy, P., Fauchard, C., 2020.
475 Geoscientists in the sky: unmanned aerial vehicles responding to geohazards. *Surv.*
476 *Geophys.* 41, 1285–1321.
477 Ayachit, U., 2015. *The ParaView Guide: A Parallel Visualization Application*. Kitware, Inc., Clifton
478 Park, NY, USA.

479 Batayneh, A., Khataibeh, J., Alrshdan, H., Tobasi, U., Al-Jahed, N., 2007. The use of microgravity,
480 magnetometry and resistivity surveys for the characterization and preservation of an
481 archaeological site at Umm er-Rasas, Jordan. *Archaeol. Prospect.* 14, 60–70.
482 <https://doi.org/10.1002/arp.301>

483 Bianchini Ciampoli, L., Santarelli, R., Loreti, E.M., Ten, A., Benedetto, A., 2023. Structural
484 detailing of buried Roman baths through GPR inspection. *Archaeol. Prospect.* 30, 3–11.
485 <https://doi.org/10.1002/arp.1776>

486 Cafiso, F., Canzoneri, A., Capizzi, P., Carollo, A., Martorana, R., Romano, F., 2023. Joint
487 interpretation of electrical and seismic data aimed at modelling the foundation soils of
488 the Maredolce monumental complex in Palermo (Italy). *Archaeol. Prospect.* 30, 69–85.
489 <https://doi.org/10.1002/arp.1803>

490 Carré, F. (Ed.), 2011. *L'archéologie en Haute-Normandie, Bilan des connaissances: Le haut*
491 *Moyen Âge.* Presses universitaires de Rouen et du Havre.
492 <https://doi.org/10.4000/books.purh.5101>

493 CloudCompare [GPL software]., 2016.

494 Cooper, D., Kay, S., Pomar, E., 2023. Reassessing Italian Renaissance church interiors through
495 non-invasive survey, in: *Advances in On- and Offshore Archaeological Prospection.*
496 *Universitätsverlag Kiel | Kiel University Publishing, Kiel, pp. 155–158.*
497 <https://doi.org/10.38072/978-3-928794-83-1/p29>

498 Dabas, M., Ollivier, J., 2021. The Ancient Rural Settlement of Plantades in Salviac (Lot, France):
499 Comparison of Previous Data with Two Geophysical Surveys. *ArcheoSciences* 45–1, 43–
500 46. <https://doi.org/10.4000/archeosciences.8319>

501 Daoust, J., 1969. Veules-les-Roses Blosseville-sur-Mer Sotteville-sur-Mer. *Études Normandes* 70,
502 1–24. <https://doi.org/10.3406/etnor.1969.3017>

503 Desrioux, L., 2018. *Notre-Dame-du-Val - Etude documentaire historique.*

504 Dubbini, M., Curzio, L.I., Campedelli, A., 2016. Digital elevation models from unmanned aerial
505 vehicle surveys for archaeological interpretation of terrain anomalies: case study of the
506 Roman castrum of Burnum (Croatia). *J. Archaeol. Sci. Rep.* 8, 121–134.
507 <http://dx.doi.org/10.1016/j.jasrep.2016.05.054>

508 Erlande-Brandenburg, A., 1966. Églises romanes en Normandie. *Bull. Monum.* 124, 289–291.

509 Evangelista, L., Silva, F. de, d'Onofrio, A., Fiore, V.D., Silvestri, F., Santolo, A.S. di, Cavuoto, G.,
510 Punzo, M., Tarallo, D., 2017. Application of ERT and GPR geophysical testing to the
511 subsoil characterization of cultural heritage sites in Napoli (Italy). *Measurement* 104,
512 326–335. <https://doi.org/10.1016/j.measurement.2016.07.042>

513 Fabian Welc, A.K., Radosław Mieszkowski, Goranka Lipovac Vrkljan, 2017. An Attempt to
514 Integration of Different Geophysical Methods (Magnetic, GPR and ERT); A Case Study
515 From the Late Roman Settlement On the Island of Rab in Croatia. *Stud. Quat.* 34, 47–59.
516 <https://doi.org/10.1515/squa-2017-0004>

517 Fajon, P., 1993. “La Chapelle du Val” de Sotteville-sur-Mer. *Connaiss. Dieppe Sa Région* 15–17.

518 Fauchard, C., Guilbert, V., Antoine, R., Ledun, C., Beaucamp, B., Maquaire, O., Costa, S.,
519 Medjkane, M., Roulland, T., 2023. Diachronic UAV study of coastal badlands supported
520 by geophysical imaging in the context of accelerated erosion processes. *Landslides.*
521 <https://doi.org/10.1007/s10346-022-02006-2>

522 Fauchard, C., Saley, A.D., Camerlynck, C., Fargier, Y., Antoine, R., Thérain, P.-F., 2018. Discovery

523 of the Romanesque church of the Abbey of our lady of Bec (Le Bec-Hellouin, Normandy,
524 France) by means of geophysical methods. *Archaeol. Prospect.* 25, 315–328.

525 Gibson, P.J., George, D.M., 2006. Geophysical investigation of the site of the former monastic
526 settlement, Clonard, County Meath, Ireland. *Archaeol. Prospect.* 13, 45–56.
527 <https://doi.org/10.1002/arp.265>

528 Giordan, D., Adams, M.S., Aicardi, I., Alicandro, M., Allasia, P., Baldo, M., De Berardinis, P.,
529 Dominici, D., Godone, D., Hobbs, P., Lechner, V., Niedzielski, T., Piras, M., Rotilio, M.,
530 Salvini, R., Segor, V., Sotier, B., Troilo, F., 2020. The use of unmanned aerial vehicles
531 (UAVs) for engineering geology applications. *Bull. Eng. Geol. Environ.* 79, 3437–3481.
532 <https://doi.org/10.1007/s10064-020-01766-2>

533 Guibert, P., Sapin, C., 2010. Groupement de recherche européen (GdRE) du CNRS«Terres cuites
534 architecturales et nouvelles méthodes de datation», bilan 2009. *Bull. Cent. D'études
535 Médiév. D'Auxerre* 77–82. <https://doi.org/10.4000/cem.11606>

536 Guilbert, V., Antoine, R., Heinkelé, C., Maquaire, O., Costa, S., Gout, C., Davidson, R., Sorin, J.-L.,
537 Beaucamp, B., Fauchard, C., 2020. FUSION OF THERMAL AND VISIBLE POINT CLOUDS :
538 APPLICATION TO THE VACHES NOIRES LANDSLIDE, NORMANDY, FRANCE. *ISPRS - Int.
539 Arch. Photogramm. Remote Sens. Spat. Inf. Sci.* XLIII-B2-2020, 227–232.
540 <https://doi.org/10.5194/isprs-archives-XLIII-B2-2020-227-2020>

541 Karamitrou, A., Bogiatzis, P., Tsokas, G.N., 2020. Fusion of geophysical images in the study of
542 archaeological sites. *Archaeol. Prospect.* 27, 119–133. <https://doi.org/10.1002/arp.1766>

543 Karamitrou, A., Tsokas, G.N., Kaimaris, D., Dadaki, S., Stampolidis, A., Vargemezis, G., Tsourlos,
544 P., Fikos, E., 2021. Joint Interpretation of Various Geophysical Data by Means of Image
545 Fusion in Philippi in Northern Greece. *ArchéoSciences* 259–262.
546 <https://doi.org/10.4000/archeosciences.9954>

547 Kvamme, K.L., Ernenwein, E.G., Menzer, J.G., 2019. Chapter 9 - Putting it all together:
548 Geophysical data integration, in: Persico, R., Piro, S., Linford, N. (Eds.), *Innovation in
549 Near-Surface Geophysics*. Elsevier, pp. 287–339. <https://doi.org/10.1016/B978-0-12-812429-1.00009-X>

551 Leucci, G., 2002. Ground-penetrating radar survey to map the location of buried structures
552 under two churches. *Archaeol. Prospect.* 9, 217–228. <https://doi.org/10.1002/arp.198>

553 Linck, R., Stele, A., Gericke, T., 2023. Reconstructing a Romanesque church based on GPR
554 results, in: *Advances in On- and Offshore Archaeological Prospection, Advances in On-
555 and Offshore Archaeological Prospection*. Universitätsverlag Kiel | Kiel University
556 Publishing, Kiel, pp. 171–174. <https://doi.org/10.38072/978-3-928794-83-1/p33>

557 Malfitana, D., Leucci, G., Fragalà, G., Masini, N., Scardozzi, G., Cacciaguerra, G., Santagati, C.,
558 Shehi, E., 2015. The potential of integrated GPR survey and aerial photographic analysis
559 of historic urban areas: A case study and digital reconstruction of a Late Roman villa in
560 Durrës (Albania). *J. Archaeol. Sci. Rep.* 4, 276–284.
561 <https://doi.org/10.1016/j.jasrep.2015.09.018>

562 Mojica, A., Pastor, L., Camerlynck, C., Florsch, N., Tabbagh, A., 2014. Magnetic Prospection of
563 the Pre-Columbian Archaeological Site of El Caño in the cultural region of Gran Coclé,
564 Panama. *Archaeol. Prospect.* 21, 201–211. <https://doi.org/10.1002/arp.1482>

565 Panisova, J., Fraštia, M., Wunderlich, T., Pašteka, R., Kušnirák, D., 2013. Microgravity and
566 Ground-penetrating Radar Investigations of Subsurface Features at the St Catherine's

567 Monastery, Slovakia. *Archaeol. Prospect.* 20, 163–174. <https://doi.org/10.1002/arp.1450>

568 Panisova, J., Murín, I., Pašteka, R., Haličková, J., Brunčák, P., Pohánka, V., Papčo, J., Milo, P.,
569 2016. Geophysical fingerprints of shallow cultural structures from microgravity and GPR
570 measurements in the Church of St. George, Svätý Jur, Slovakia. *J. Appl. Geophys.* 127,
571 102–111. <https://doi.org/10.1016/j.jappgeo.2016.02.009>

572 Panisova, J., Pašteka, R., Papčo, J., Fraštia, M., 2012. The calculation of building corrections in
573 microgravity surveys using close range photogrammetry. *Surf. Geophys.*
574 <https://doi.org/10.3997/1873-0604.2012034>

575 Panissod, C., Dabas, M., Florsch, N., Hesse, A., Jolivet, A., Tabbagh, A., Tabbagh, J., 1998.
576 Archaeological prospecting using electric and electrostatic mobile arrays. *Archaeol.*
577 *Prospect.* 5, 239–251. [https://doi.org/10.1002/\(SICI\)1099-0763\(199812\)5:4<239::AID-](https://doi.org/10.1002/(SICI)1099-0763(199812)5:4<239::AID-)
578 [ARP106>3.0.CO;2-N](https://doi.org/10.1002/(SICI)1099-0763(199812)5:4<239::AID-ARP106>3.0.CO;2-N)

579 Papadopoulos, N., Sarris, A., Maria, C., Salvi, Déderix, S., Soupios, P., Dikmen, Ü., 2012.
580 Rediscovering the small theatre and amphitheatre of ancient Ierapytna (SE Crete) by
581 integrated geophysical methods. *J. Archaeol. Sci.* 39.
582 <https://doi.org/10.1016/j.jas.2012.01.044>

583 Papadopoulos, N., Tsokas, G., Sarris, A., Tsourlos, P., Vargemezis, G., 2014. Ground-based
584 archaeological prospection: Case studies from Greece. *First Break.*
585 <https://doi.org/10.3997/1365-2397.32.8.76966>

586 Papadopoulos, N.G., Yi, M.-J., Kim, J.-H., Tsourlos, P., Tsokas, G.N., 2010. Geophysical
587 investigation of tumuli by means of surface 3D Electrical Resistivity Tomography. *J. Appl.*
588 *Geophys.* 70, 192–205. <https://doi.org/10.1016/j.jappgeo.2009.12.001>

589 Pašteka, R., Zahorec, P., 2000. Interpretation of microgravimetric anomalies in the region of
590 the former church of St. Catherine, Dechtice. *Contrib. Geophys. Geod.* 30, 373–387.

591 Pierrot Deseilligny, M., Clery, I., 2011. APERO, AN OPEN SOURCE BUNDLE ADJUSTMENT
592 SOFTWARE FOR AUTOMATIC CALIBRATION AND ORIENTATION OF SET OF IMAGES. *Int.*
593 *Arch. Photogramm. Remote Sens. Spat. Inf. Sci.* XXXVIII-5/W16, 269–276.
594 <https://doi.org/10.5194/isprsarchives-XXXVIII-5-W16-269-2011>

595 Pierrot-Deseilligny, M., Clery, I., 2012. Some possible protocols of acquisition for optimal use of
596 the “APER0” open source software in automatic orientation and calibration, in:
597 *Castelldefels, Spain, Tutorial, EuroCOW Workshop.* pp. 8–10.

598 Pomar, E., Kay, S., Campbell, P., Vuković, K., 2023. Integrated GPR and laser scanning of Piazza
599 Sant’Anastasia, Rome, in: *Non-Intrusive Methodologies for Large Area Urban Research.*
600 *Archaeopress Archaeology, Oxford,* pp. 94–98.

601 Rabbel, W., Erku, E., Stümpel, H., Wunderlich, T., Pašteka, R., Papco, J., Niewöhner, P., Bariş, Ş.,
602 Çakin, O., Pekşen, E., 2015. Discovery of a Byzantine Church in Iznik/Nicaea, Turkey: an
603 Educational Case History of Geophysical Prospecting with Combined Methods in Urban
604 Areas. *Archaeol. Prospect.* 22, 1–20. <https://doi.org/10.1002/arp.1491>

605 Ranieri, G., Godio, A., Loddo, F., Stocco, S., Casas, A., Capizzi, P., Messina, P., Orfila, M., Cau,
606 M.A., Chávez, M.E., 2016. Geophysical prospection of the Roman city of Pollentia,
607 Alcúdia (Mallorca, Balearic Islands, Spain). *J. Appl. Geophys.* 134, 125–135.
608 <https://doi.org/10.1016/j.jappgeo.2016.08.009>

609 Sapin, C., Baylé, M., Büttner, S., Guibert, P., Blain, S., Lanos, P., Chauvin, A., Dufresne, P.,
610 Oberlin, C., 2008. *Archéologie du bâti et archéométrie au Mont-Saint-Michel, nouvelles*

611 approches de Notre-Dame-sous-Terre. *Archéologie Médiév.* 71–122.
612 <https://doi.org/10.4000/archeomed.21054>

613 Tabbagh, A., 2018. La prospection : évolution de la sous-discipline, évolution du métier.
614 *ArcheoSciences* 42–1, 103–108. <https://doi.org/10.4000/archeosciences.5440>

615 Tabuteau, B., 2019. Lepers and leper-houses in eastern Normandy and the Vexin in the 13th
616 century according to the diary of pastoral visits by Eudes Rigaud, archbishop of Rouen,
617 *Lépreux et léproseries en Normandie orientale et Vexin au XIIIe siècle d'après le journal*
618 *des visites pastorales d'Eudes Rigaud, archevêque de Rouen. Rev. Hist. L'Église Fr.*

619 Telford, W.M., Geldart, L.P., Sheriff, R.E., 1990. *Applied Geophysics*, 2nd ed. Cambridge
620 University Press, Cambridge. <https://doi.org/10.1017/cbo9781139167932>

621 Trinks, I., Hinterleitner, A., Neubauer, W., Nau, E., Löcker, K., Wallner, M., Gabler, M., Filzwieser,
622 R., Wilding, J., Schiel, H., Jansa, V., Schneidhofer, P., Trausmuth, T., Sandici, V., Ruß, D.,
623 Flöry, S., Kainz, J., Kucera, M., Vonkilch, A., Tencer, T., Gustavsen, L., Kristiansen, M., Bye-
624 Johansen, L.-M., Tønning, C., Zitz, T., Paasche, K., Gansum, T., Seren, S., 2018. Large-area
625 high-resolution ground-penetrating radar measurements for archaeological prospection.
626 *Archaeol. Prospect.* 25, 171–195. <https://doi.org/10.1002/arp.1599>

627 Tsokas, G.N., Tsourlos, P.I., Vargemezis, G., Novack, M., 2008. Non-destructive electrical
628 resistivity tomography for indoor investigation: the case of Kapnikarea Church in Athens.
629 *Archaeol. Prospect.* 15, 47–61. <https://doi.org/10.1002/arp.321>

630 Viberg, A., Schultzen, J., Wikström, A., 2013. RECONSTRUCTING THE SPATIAL LAYOUT OF THE
631 CHURCH OF ST. LAWRENCE, SIGTUNA, SWEDEN USING GROUND-PENETRATING RADAR
632 AND PHOTOGRAMMETRY, in: *Archaeological Prospection*. Verlag der österreichischen
633 Akademie der Wissenschaften, Vienna, pp. 74–76. <https://doi.org/10.2307/j.ctvjsf630.28>

634 Wasylyszyn, N., 2018. *L'Église Saint-Martin à Armentières-sur-Avre : histoire et architecture*.
635 Confluence, Patrimoine méconnu. Autour de Verneuil en Pays d'Avre et d'Iton 31–41.

636 Wasylyszyn, N., 2006. *Inventaire et observations sur les églises Romanes précoces de Haute-*
637 *Normandie (Xe-XIe siècles)*. Haute Normandie Archéologique XIII.

638 Welc, F., Mieszkowski, R., Vrkljan, G.L., Konestra, A., 2017. An Attempt to Integration of
639 Different Geophysical Methods (Magnetic, GPR and ERT); A Case Study From the Late
640 Roman Settlement On the Island of Rab in Croatia. *Stud. Quat.* 34, 47–59.

641 Wilken, D., Jürgens, F., Erkul, E., Rabbel, W., Müller, U., 2023. Deal with steel: investigating the
642 wreck of the heavy cruiser Admiral Scheer, in: *Advances in On- and Offshore*
643 *Archaeological Prospection*. Universitätsverlag Kiel | Kiel University Publishing, Kiel, pp.
644 71–75. <https://doi.org/10.38072/978-3-928794-83-1/p12>

645 Wilken, D., Wunderlich, T., Hollmann, H., Schwardt, M., Rabbel, W., Mohr, C., Schulte-Kortnack,
646 D., Nakoinz, O., Enzmann, J., Jürgens, F., Wilkes, F., 2019. Imaging a medieval shipwreck
647 with the new PingPong 3D marine reflection seismic system. *Archaeol. Prospect.* 26,
648 211–223. <https://doi.org/10.1002/arp.1735>

649
650